Letter Vol. 6, No. 1 / January 2019 / Optica 111

# Super-octave longwave mid-infrared coherent transients produced by optical rectification of few-cycle 2.5-μm pulses

Sergey Vasilyev,[1,*] Igor S. Moskalev,[1] Viktor O. Smolski,[1] Jeremy M. Peppers,[1] Mike Mirov,[1] Andrey V. Muraviev,[3] Kevin Zawilski,[4] Peter G. Schunemann,[4] Sergey B. Mirov,[1,5] Konstantin L. Vodopyanov,[3] and Valentin P. Gapontsev[2]

[1]IPG Photonics—Southeast Technology Center, 100 Lucerne Ln., Birmingham, Alabama 35211, USA
[2]IPG Photonics Corporation, 50 Old Webster Rd, Oxford, Massachusetts 01540, USA
[3]CREOL, College of Optics and Photonics, University of Central Florida, Orlando, Florida 32816, USA
[4]BAE Systems, P.O. Box 868, MER15-1813, Nashua, New Hampshire 03061, USA
[5]Department of Physics, University of Alabama at Birmingham, 1530 3rd Ave S, Birmingham, Alabama 35294, USA
*Corresponding author: svasilyev@ipgphotonics.com

Received 19 October 2018; revised 2 December 2018; accepted 2 December 2018 (Doc. ID 348651); published 17 January 2019

**Femtosecond laser sources and optical frequency combs in the molecular fingerprint region of the electromagnetic spectrum are crucial for a plethora of applications in natural and life sciences. Here we introduce $Cr^{2+}$-based lasers as a convenient means for producing super-octave mid-IR electromagnetic transients via optical rectification (or intra-pulse difference frequency generation, IDFG). We demonstrate that a relatively long, 2.5 μm, central wavelength of a few-cycle $Cr^{2+}$:ZnS driving source (20 fs pulse duration, 6 W average power, 78 MHz repetition rate) enabled the use of highly nonlinear $ZnGeP_2$ crystal for IDFG with exceptionally high conversion efficiency (>3%) and output power of 0.15 W, with the spectral span of 5.8–12.5 μm. Even broader spectrum was achieved in GaSe crystal: 4.3–16.6 μm for type I and 5.8–17.6 μm for type II phase matching. The results highlight the potential of this architecture for ultrafast spectroscopy and generation of broadband frequency combs in the longwave infrared.** 

https://doi.org/10.1364/OPTICA.6.000111

Few-cycle laser sources with a spectral span exceeding an octave in the longwave portion of the mid-IR spectrum (5–20 μm, 15–60 THz) are vital for a number of applications, ranging from molecular fingerprinting with dual optical frequency combs [1], IR nano-imaging [2], Fourier transform infrared nanospectroscopy (nano-FTIR) absorption spectroscopy [3], time-resolved optical spectroscopy, and studies of ultrafast dynamics [4,5] to high-field science [6].

In the past decade, super-octave longwave mid-IR pulses have been generated by a number of techniques. One popular approach is based on spectral broadening of femtosecond (fs) sources. Remarkable examples include supercontinuum generation (SCG) in chalcogenide fibers driven by an optical parametric amplifier (OPA) [7], and augmentation of the OPA spectrum by SCG via cascaded quadratic nonlinearities in crystals [8]. Another large family of super-octave mid-IR sources is based on frequency divide-by-2 (subharmonic) optical parametric oscillators (OPOs) that feature broad bandwidth, low pumping thresholds [9], high conversion efficiency [10], and the capability to scale the average power of an octave-spanning output to watt level [11]. Notably, subharmonic OPOs fully preserve coherence of the pump by dividing its carrier–envelope offset frequency ($f_{CEO}$) exactly by two [12,13]. Yet, since a subharmonic OPO spectrum is centered at twice the pump wavelength, stretching its output spectra beyond 10 μm with currently available lasers is challenging due to limitations set by the group velocity dispersion in the OPO cavity.

Alternatively, fs longwave mid-IR pulses with super-octave spectra can be produced in a significantly simplified scheme, namely, optical rectification (which is equivalent to intra-pulse difference frequency generation, IDFG) [14–16]. In the time domain, a few-cycle pulse creates nonlinear (NL) polarization in a NL $\chi^{(2)}$ crystal, resulting in forward emission of longwave mid-IR light with an optical period on the order of the pump pulse duration. In the frequency domain, this corresponds to difference frequency generation between spectral components within the same pump pulse. Thus, $f_{CEO}$ of the pump field is subtracted out providing an offset-free mid-IR comb consisting of exact harmonics of the laser repetition rate ($f_R$). In many respects, IDFG and OPO techniques are complementary: the IDFG provides access to the long-wavelength part of the mid-IR, which is adjacent to the typical spectral coverage of a subharmonic OPO.

To produce IDFG transients in the mid-IR, one needs relatively broadband pump pulses with a few-optical-cycle duration. Typically, this comes at the expense of an additional (usually fiber based) stage for NL broadening and post compression of pulses from a relatively narrowband mode-locked driving laser. The key

**Table 1. Parameters of Selected IDFG Sources**

| Pump λ (μm) | Pulse Width (fs)[a] | Pump Average Power (W)[a] | NL Crystal | IDFG Average Power (mW) | IDFG Spectral Span (μm) | Conversion Efficiency[b] | Ref. |
|---|---|---|---|---|---|---|---|
| 1.03 | 250 (19) | 90 (50) | LGS | 103 | 6.8–16.4 | $1.1 \cdot 10^{-3}$ | [17] |
| 1.57 | 270 (11) | 0.35 (0.25) | OP-GaP | 0.25 | 4–12 | $7.1 \cdot 10^{-4}$ | [1] |
| 2.09 | 260 (15) | 19 (7) | GaSe | 24 | 4.4–20 | $1.3 \cdot 10^{-3}$ | [18] |
| 1.95[c] | 110 (16) | 37 (32) | GaSe | 450 | 6–18 | $1.4 \cdot 10^{-2}$ | [19] |
| 2.5 | 20 | 5.9 | GaSe | 13 | 4.3–16.6, 5.8–17.6 | $2.2 \cdot 10^{-3}$ | [d] |
| 2.5 | 20 | 4.5 | ZGP | 148 | 5.8–12.5 | $3.3 \cdot 10^{-2}$ | [d] |

[a]Before and after (in brackets) pulse compression.
[b]Measured with respect to the original laser power before compression.
[c]High-energy low repetition rate (1.25 MHz) Tm:FCPA system.
[d]This paper.

parameters of several advanced longwave mid-IR IDFG setups [1,17–19] are summarized in Table 1.

The efficiency of the IDFG process scales in a similar fashion as THz generation via optical rectification [20]. An important scaling rule is quadratic dependence on the effective interaction length ($L_{\text{eff}}$), which is limited mainly by the group velocity mismatch between pump and mid-IR pulses. In most NL crystals, this mismatch narrows down when the pump wavelength increases (it becomes closer to that of the IDFG output). For example, in GaSe crystal, assuming IDFG center wavelength ~10 μm and pump pulse duration 15 fs, $L_{\text{eff}} = 22$ μm for 1 μm pump and as large as 1.5 mm for 2.5 μm pump. With the $L_{\text{eff}}^2$ scaling, shifting to a longer wavelength pump gives an almost 5,000 times increase in IDFG conversion efficiency. Yet another crucial advantage of long-wavelength pumping is access to NL materials with broad mid-IR transparency and high figure of merit. Moreover, decreased energy of pump photons greatly reduces the parasitic effects arising from multi-photon absorption.

Here we report on super-octave wide coherent longwave mid-IR transients produced via IDFG with a mode-locked $Cr^{2+}$:ZnS laser system with wavelength centered at 2.5 μm. Most importantly, the pumping well above 2 μm has enabled the use of highly efficient $ZnGeP_2$ (ZGP) crystal. Further, we benefit from a unique blend of physical, laser, and NL optical parameters of polycrystalline $Cr^{2+}$:ZnS that allows for direct generation and amplification of few-cycle pulses in the range of 2–3 μm [21,22]. The main advantages of this laser medium include: very broad spectral bandwidth (1.8–3.3 μm), high laser gain, and high Kerr coefficient. It has been demonstrated that a simple and robust, yet efficient, single-pass arrangement of polycrystalline $Cr^{2+}$:ZnS amplifiers enables simultaneous amplification of pulses to multi-watt level, broadening of their spectrum, and shortening of pulse duration to 2–3 optical cycles [21,22].

A schematic of our IDFG setup is illustrated in Fig. 1. The design of the driving laser is very similar to those described in [21,23]. In short, we couple 1.3 W output of a 3-cycle Kerr-lens mode-locked $Cr^{2+}$:ZnS oscillator to a single-pass $Cr^{2+}$:ZnS amplifier at a full repetition rate $f_R = 78$ MHz. Both the oscillator and amplifier are optically pumped at 1567 nm by radiation of commercial continuous wave (cw) Er-doped fiber lasers (EDFLs). The source is enclosed in a dust-tight 18″ × 24″ case and purged with dry air. The improvements over the system from [23] include: slightly increased spectral bandwidth of the oscillator, better dispersion control between the oscillator and amplifier stages, and better spatial mode matching. Also, we equipped the oscillator with a commercial kit for $f_R$ stabilization (based on a phase-locked loop controller) and used a low-noise single-frequency EDFL to pump the oscillator.

The spectral and temporal characteristics of the 2.5 μm driving laser are illustrated in Fig. 2. The measurements were performed during a gradual increase of laser power after the amplifier, from initial 1.2 W to 5.9 W, as marked in Fig. 2(c). To evaluate the pulse duration, we used a second-order interferometric autocorrelator (IAC) with two-photon detection. We used a set of five dichroic mirrors to suppress the second harmonic (SH) and higher optical harmonics produced in the polycrystalline gain element due to random quasi-phase matching [24,25]. The IAC measurements were possible up to 5.2 W of output power [the corresponding spectrum is marked in Fig. 2(c) by an asterisk]. At higher powers, the output was too contaminated by residual near-IR radiation. We conservatively estimate 20 fs pulse duration (2.4 cycles) at the maximum 5.9 W output power. The measured pulse durations $\tau^{(AC)}$ exceed the limits $\tau^{(S)}$ derived from the spectra by 30–40%. We partly explain this difference by a significant uncompensated third-order dispersion (TOD ≈ 8000 $fs^3$). Overall, we obtained sub-3-cycle pulses at 2.5 μm central wavelength with 75 nJ energy and 3.3 MW peak power at 78 MHz repetition rate. The conversion efficiency from cw EDFL radiation to few-cycle middle IR pulses reached 22%.

We locked the oscillator to $f_R = 77.92505$ MHz. We then characterized the stability of the laser pulse train by analyzing the signal from a fast (1.8 GHz bandwidth) InGaAs photodetector with a radio frequency (RF) spectrum analyzer. The RF spectra measured with two different resolution bandwidths (RBWs) are shown in Fig. 3. Using the procedure described in [26,27], we estimated the relative root-mean-square pulse energy fluctuations to be $<5 \cdot 10^{-4}$ and the relative time jitter (with respect to the pulse

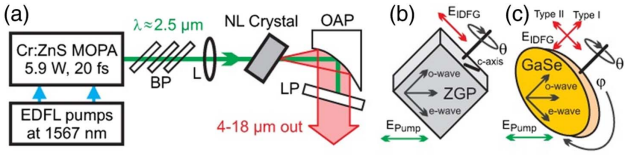


**Fig. 1.** (a) Schematic of the IDFG setup. MOPA, fs $Cr^{2+}$:ZnS master oscillator power amplifier system centered at ~2.5 μm; EDFL, pump lasers with 6.5 W power for the oscillator and up to 20 W for the amplifier stage; BP, a set of Brewster plates for fine-tuning of the temporal parameters of output pulses; L, AR-coated $CaF_2$ focusing lens $f =$ 100 mm; OAP, gold-coated 90° off-axis parabola with RFL = 50 mm; LP, long-pass filter. (b) ZGP and (c) GaSe crystals' orientations.

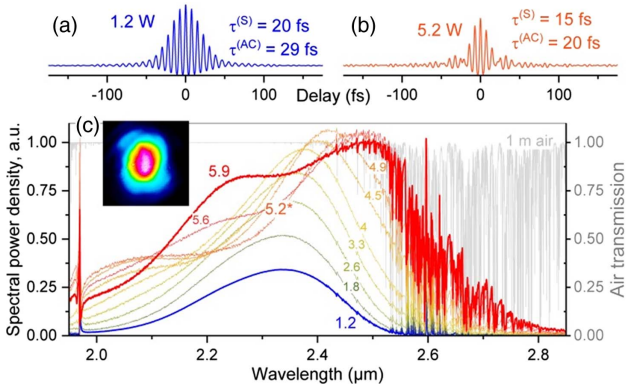


**Fig. 2.** (a), (b) Interferometric autocorrelator (IAC) traces for output powers of 1.2 W and 5.2 W. $\tau^{(IAC)}$ and $\tau^{(S)}$ are corresponding pulse widths derived from the IACs ($sech^2$ fit) and from the spectra (assuming a flat spectral phase). (c) Spectra of the driving laser were acquired during the gradual increase of MOPA power from 1.2 W to 5.9 W. The final spectrum is normalized to unity, which corresponds to the spectral power density 12 mW/nm. The inset shows the output beam profile at 5.9 W power. The laser enclosure and OSA were purged by dry air, and approximately 1 m path between the enclosure and the OSA was at 46% relative humidity. Transmission of 1 m of standard air is shown in gray (HITRAN simulation).

period) to be $<10^{-5}$. The obtained estimates are approximate and conservative, as we detected the laser intensity at its SH wavelength.

The IDFG experiments were carried out using two nonlinear crystals: ZGP and GaSe. The ZGP sample was antireflection (AR) coated, 3 mm thick, and cut for type I phase matching. The integral transmission of the sample was 94% and 87% over the 2–2.8 μm and 7–11 μm spectral bands, respectively. The GaSe sample was uncoated and ≈1 mm thick. The natural cleavage of GaSe along (001) plane (*z*-cut) allows for both types of phase matching [28]. To satisfy the phase-matching condition, one has to provide both ordinary (*o*) and extraordinary (*e*) polarized components of the pump electric field (*E*-field). For this purpose, both ZGP and GaSe crystals were oriented, such that the polarization vector of the pump *E*-field had approximately equal *o* and *e* components [Figs. 1(b) and 1(c)]. The pump beam was focused to a NL crystal by a plano-convex $f = 100$ mm lens to a spot size of about 75 μm ($1/e^2$ intensity radius). The output radiation was collimated by an off-axis parabola and separated from the driving pulses by a set of long-pass (LP) filters.

The IDFG outputs were optimized for the highest average power measured behind a LP filter transmitting at >6.7 μm. Optimizations included: translation of the NL crystal along the focused driving beam and selection of the right combination of

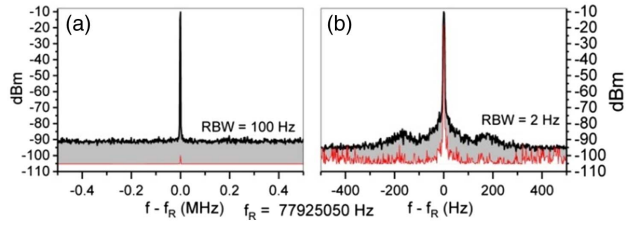


**Fig. 3.** RF power spectra of fs pulse train detected at the laser second-harmonic wavelength with two resolution bandwidths (RBW). $f_R = 77925050$ Hz.

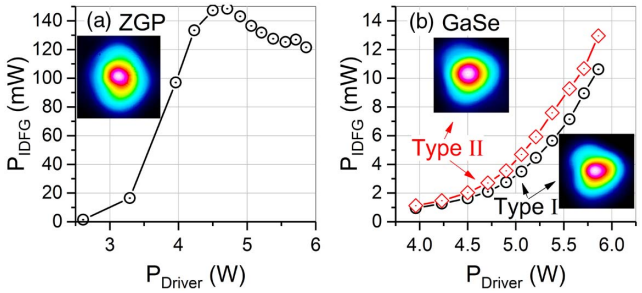


**Fig. 4.** Average power of the IDFG signal ($P_{IDFG}$) versus average power of the driving laser in (a) ZGP and (b) GaSe crystals. The insets show the profiles of output beam acquired at $P_{Driver} = 5.9$ W. The measurements were carried out behind a 6.7 μm LP with 89% (74%) integral transmission over 7–12 μm (6–15 μm) band.

Brewster plates for pre-chirping of input pulses. The IDFG output versus input power dependence for ZGP and GaSe is shown in Fig. 4. One can see that for both crystals there are ranges with very steep, stronger than quadratic, dependence. This can be explained by the fact that the driving pulses experience significant spectral broadening that depends on the amplifier gain, thus boosting the steepness of the dependence. An additional experiment with a set of neutral filters, which was carried out at constant amplifier gain, has confirmed the theoretical quadratic dependence.

The IDFG spectra obtained with the ZGP sample (type I phase matching with polar and azimuthal angles $\theta \approx 50°$ and $\phi \approx 0°$, correspondingly) are shown in Fig. 5(a). The spectra span over an octave, 5.8–12.5 μm when measured at −30 dB level with respect to the maximum. Figure 5(a) also compares two spectra, which were measured at different power levels (and hence different bandwidths) of the driving pulses.

The maximum IDFG output power of 150 mW was measured at 4.5 W average power of the driving pulses with 16 THz FWHM

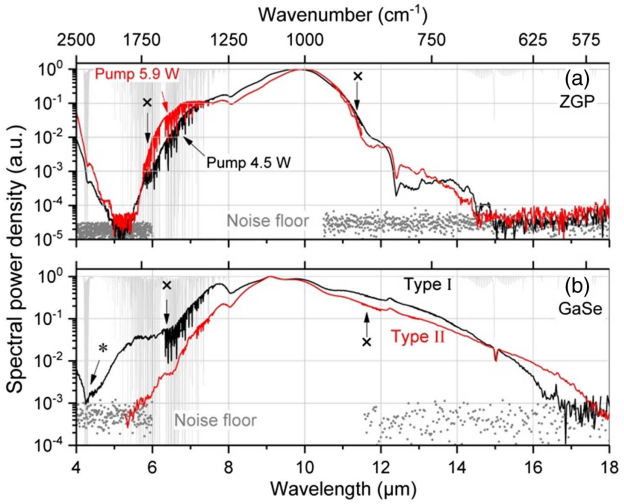


**Fig. 5.** Normalized IDFG spectra: (a) Obtained from ZGP at 4.5-W (black line) and 5.9-W (red line) pump. The spectral power density at the peak was 76 μW/nm and 71 μW/nm, respectively. (b) Obtained from GaSe for type I and type II phase-matching at 5.9 -W pump, with the peak IDFG spectral density of 3.1 μW/nm and 5.2 μW/nm, respectively. Scattered dots show the noise floor. Gray background shows transmission of 1 m standard air.

bandwidth. The increase in input power to 5.9 W (27 THz bandwidth) resulted in a roll-off of IDFG power to 120 mW. A probable contributor to the roll-off is NL absorption of the pump (the 3.8 MW peak power corresponds to $\sim 4 \cdot 10^{10}$ W/cm$^2$ intensity in the focus). Nevertheless, to the best of our knowledge, we achieved, by far, the highest reported to date IDFG efficiency that exceeds 3%. Taking into account surface reflection losses in ZGP and 25% losses in the LP filter, we estimate 5.2% internal efficiency, which corresponds to 21% quantum efficiency.

The GaSe crystal provided much broader spectrum approaching two octaves [Fig. 5(b)], although at the expense of a 10-fold decrease in the IDFG power [Fig. 4(b)]. The instantaneous spectral span we measured with GaSe at −30 dB level was 4.3–16.6 μm for type I ($\theta \approx 11.3°$, $\phi \approx 90°$) and 5.8–17.6 μm for type II phase matching ($\theta \approx 12.6°$, $\phi \approx 0°$), with type I providing somewhat broader spectrum (and slightly shorter central wavelength). It is probable that the spectrum obtained for type II phase matching extends beyond 18 μm (see, e.g., [18]). However we cannot confirm it due to the limited sensitivity of our spectroscopic setup. Remarkably, we observed an overlap between the longwave tail of the driving laser spectrum and the short-wave tail of the IDFG spectrum [this point is marked in Fig. 5(b) by an asterisk]. This feature has enabled direct detection of the $f_{\mathrm{CEO}}$ of the pump through measuring a beat note between the pump and the IDFG output (however, this will be the topic of a separate paper).

In conclusion, we demonstrate efficient generation of coherent longwave mid-IR transients using, as a pump, a compact 2.5 μm MOPA laser system that directly produces <20 fs pulses without external pulse compression. ZGP is ideally suited for the generation of an octave-wide spectrum (5.8–12.5 μm) with an output power of 0.15 W and record-high optical conversion efficiency of 3%, while GaSe allows, with types I and II phase matching, to cover 2 octaves in the mid-IR (4.3–17.6 μm), although with lower (13 mW) output power. The roll-off of the IDFG output power in ZGP and the limitations on the average power and pulse energy achievable via IDFG are yet to be explored. However, it is likely that the output power of GaSe-based IDFG could be scaled to sub-watt level, due to recent breakthroughs in power-scaling of few-cycle $Cr^{2+}$-based lasers to >25 W [29]. Finally, since the IDFG produces an offset-free comb of frequencies, with a locked repetition rate of the driving laser, the described setup might find numerous applications in spectroscopy, in particular in dual-comb spectroscopy with conventional (using square-law detectors) as well as electro-optic sampling [30]. A similar laser architecture can be used with the driver systems with much higher pulse energies at lower repetition rates [19, 21].

**Funding.** Office of Naval Research (ONR) (N00014-15-1-2659, N00014-17-1-2705); Defense Advanced Research Projects Agency (DARPA) (W31P4Q-15-1-0008); U.S. Department of Energy (DOE) (DE-SC0018378).

**Acknowledgment.** S. B. M declares competing financial interests. A. V. M. and K. L. V. acknowledge support from the Office of Naval Research (ONR) and from the Defense Advanced Research Projects Agency (DARPA). S. B. M. also acknowledges support from DARPA as well as from the Department of Energy (DOE).

## REFERENCES

1. H. Timmers, A. Kowligy, A. Lind, F. C. Cruz, N. Nader, M. Silfies, G. Ycas, T. K. Allison, P. G. Schunemann, S. B. Papp, and S. A. Diddams, Optica **5**, 727 (2018).
2. Z. Fei, A. S. Rodin, G. O. Andreev, W. Bao, A. S. McLeod, M. Wagner, L. M. Zhang, Z. Zhao, M. Thiemens, G. Dominguez, M. M. Fogler, A. H. Castro Neto, C. N. Lau, F. Keilmann, and D. N. Basov, Nature **487**, 82 (2012).
3. F. Huth, A. Govyadinov, S. Amarie, W. Nuansing, F. Keilmann, and R. Hillenbrand, Nano Lett. **12**, 3973 (2012).
4. A. J. Fleisher, B. J. Bjork, T. Q. Bui, K. C. Cossel, M. Okumura, and J. Ye, J. Phys. Chem. Lett. **5**, 2241 (2014).
5. M. Wagner, A. S. McLeod, S. J. Maddox, Z. Fei, M. Liu, R. D. Averitt, M. M. Fogler, S. R. Bank, F. Keilmann, and D. N. Basov, Nano Lett. **14**, 4529 (2014).
6. J. Weisshaupt, V. Juvé, M. Holtz, S. Ku, M. Woerner, T. Elsaesser, S. Ališauskas, A. Pugžlys, and A. Baltuška, Nat. Photonics **8**, 927 (2014).
7. C. Petersen, U. Møller, I. Kubat, B. Zhou, S. Dupont, J. Ramsay, T. Benson, S. Sujecki, N. Abdel-Moneim, Z. Tang, D. Furniss, A. Seddon, and O. Bang, Nat. Photonics **8**, 830 (2014).
8. M. Seidel, X. Xiao, S. A. Hussain, G. Arisholm, A. Hartung, K. T. Zawilski, P. G. Schunemann, F. Habel, M. Trubetskov, V. Pervak, O. Pronin, and F. Krausz, Sci. Adv. **4**, eaaq1526 (2018).
9. V. O. Smolski, H. Yang, S. D. Gorelov, P. G. Schunemann, and K. L. Vodopyanov, Opt. Lett. **41**, 1388 (2016).
10. A. Marandi, K. Ingold, M. Jankowski, and R. Byer, Optica **3**, 324 (2016).
11. V. Smolski, S. Vasilyev, I. Moskalev, M. Mirov, Q. Ru, A. Muraviev, P. Schunemann, S. Mirov, V. Gapontsev, and K. Vodopyanov, Appl. Phys. B **124**, 101 (2018).
12. K. Lee, C. Mohr, J. Jiang, P. Schunemann, K. Vodopyanov, and M. Fermann, Opt. Express **23**, 26596 (2015).
13. A. Muraviev, V. Smolski, Z. Loparo, and K. L. Vodopyanov, Nat. Photonics **12**, 209 (2018).
14. A. Bonvalet, M. Joffre, J. L. Martin, and A. Migus, Appl. Phys. Lett. **67**, 2907 (1995).
15. R. Huber, A. Brodschelm, F. Tauser, and A. Leitenstorfer, Appl. Phys. Lett. **76**, 3191 (2000).
16. R. A. Kaindl, F. Eickemeyer, M. Woerner, and T. Elsaesser, Appl. Phys. Lett. **75**, 1060 (1999).
17. I. Pupeza, D. Sánchez, J. Zhang, N. Lilienfein, M. Seidel, N. Karpowicz, T. Paasch-Colberg, I. Znakovskaya, M. Pescher, W. Schweinberger, V. Pervak, E. Fill, O. Pronin, Z. Wei, F. Krausz, A. Apolonski, and J. Biegert, Nat. Photonics **9**, 721 (2015).
18. J. Zhang, K. Mak, N. Nagl, M. Seidel, D. Bauer, D. Sutter, V. Pervak, F. Krausz, and O. Pronin, Light: Sci. Appl. **7**, 17180 (2018).
19. C. Gaida, M. Gebhardt, T. Huermann, F. Stutzki, C. Jauregui, J. Antonio-Lopez, A. Schülzgen, R. Amezcua-Correa, A. Tünnermann, I. Pupeza, and J. Limpert, Light: Sci. Appl. **7**, 94 (2018).
20. K. L. Vodopyanov, Opt. Express **14**, 2263 (2006).
21. S. Mirov, I. Moskalev, S. Vasilyev, V. Smolski, V. Fedorov, D. Martyshkin, J. Peppers, M. Mirov, A. Dergachev, and V. Gapontsev, IEEE J. Sel. Top. Quantum Electron. **24**, 1601829 (2018).
22. S. Vasilyev, I. Moskalev, M. Mirov, V. Smolski, S. Mirov, and V. Gapontsev, Opt. Mater. Express **7**, 2636 (2017).
23. G. Vampa, S. Vasilyev, H. Liu, M. Mirov, P. Bucksbaum, and D. Reis, Opt. Lett. **44**, 259 (2019).
24. S. Vasilyev, I. Moskalev, M. Mirov, S. Mirov, and V. Gapontsev, Opt. Lett. **40**, 5054 (2015).
25. S. Vasilyev, I. Moskalev, M. Mirov, V. Smolski, S. Mirov, and V. Gapontsev, Proc. SPIE **9731**, 97310B (2016).
26. D. von der Linde, Appl. Phys. B **39**, 201 (1986).
27. Y. Wang, T. Fernandez, N. Coluccelli, A. Gambetta, P. Laporta, and G. Galzerano, Opt. Express **25**, 25193 (2017).
28. K. Vodopyanov, J. Opt. Soc. Am. B **10**, 1723 (1993).
29. S. Vasilyev, I. Moskalev, V. Smolski, J. Peppers, M. Mirov, S. Mirov, and V. Gapontsev, *Advanced Solid State Lasers Conference*, OSA Technical Digest (online) (Optical Society of America, 2018), paper AW3A.1.
30. A. S. Kowligy, H. Timmers, A. Lind, U. Elu, F. C. Cruz, P. G. Schunemann, J. Biegert, and S. A. Diddams, "Infrared electric-field sampled frequency comb spectroscopy," arXiv:1808.10275v2 (2018).